FEBS Letters 580 (2006) 4567–4570

Electrostatic role of the non-heme iron complex in bacterial photosynthetic reaction center

Hiroshi Ishikita[1], Ernst-Walter Knapp*

Institute of Chemistry and Biochemistry, Free University of Berlin, Takustrasse 6, D-14195 Berlin, Germany

Received 17 June 2006; revised 4 July 2006; accepted 7 July 2006

Available online 17 July 2006

Edited by Peter Brzezinski

Abstract To elucidate the role of the non-heme iron complex (Fe-complex) in the electron transfer (ET) events of bacterial photosynthetic reaction centers (bRC), we calculated redox potentials of primary/secondary quinones $Q_{A/B}$ ($E_m(Q_{A/B})$) in the Fe-depleted bRC. Removing the Fe-complex, the calculated $E_m(Q_{A/B})$ are downshifted by ~220 mV/~80 mV explaining both the 15-fold decrease in ET rate from bacteriopheophytin (H_A^-) to Q_A and triplet state occurrence in Fe-depleted bRC. The larger downshift in $E_m(Q_A)$ relative to $E_m(Q_B)$ increases the driving-energy for ET from Q_A to Q_B by 140 meV, in agreement with ~100 meV increase derived from kinetic studies.

Keywords: Non-heme iron; Redox potential; Quinone; Electron transfer; Bacterial photosynthetic reaction center; Photosystem II

1. Introduction

The primary ET event in bRC is a charge-separation process, which occurs after electronic excitation at the bacteriochlorophyll *a* (BChl*a*) dimer, the special pair (P). As a result, P becomes oxidized, while an electron is transferred along the A-branch cofactors from the accessory BChl*a* B_A via H_A to Q_A in the A-branch and subsequently to Q_B in the B-branch. After the first ET process, Q_B^- is protonated to Q_BH and stabilized by a second ET and proton transfer (PT) event, which results in the formation of the doubly protonated dihydroquinone Q_BH_2.

The non-heme iron complex (Fe-complex; referring to center Fe and its ligands) is situated equidistantly from both Q_A and Q_B (Fig. 1). Two symmetrical pairs of His residues, His-L190/His-M219 and His-L230/His-M266, and one acidic residue Glu-M234 are ligands of the Fe-complex. The two His residues of the former pair form an H bond with Q_B and Q_A, respectively. In spite of its unique position as being equidistant from Q_A and Q_B, a definite functional role of the Fe-complex is still an open question. The depletion of the Fe-complex (Fe-depleted bRC) resulted in a dramatic decrease in the forward rate of ET from H_A^- to Q_A by a factor of at least 15 [1]. The decrease in the forward ET rate enhances simultaneously the competing backward ET process, resulting in charge recombination of the $P^+H_A^-$ state, generation of triplet state and decrease in the yield of the final product $P^+Q_B^-$ state. To explain the decrease in the forward ET rate contributions of (i) structural modulation, (ii) $E_m(Q_A)$ shift, or (iii) change of vibronic coupling between H_A and Q_A were proposed [1], but the issue remained undecided. On the other hand, upon Fe depletion the rate of the ET from Q_A^- to Q_B (k_{AB}^1) decreases by only a factor of 2 [2]. Hence, the conformational gating and PT events of kinetic phase 1 are essentially not affected by Fe depletion, and the underlying ET process is still too fast to be rate limiting for kinetic phase 1. On the other hand, recent FTIR studies of Remy and Gerwert [3] suggested that Q_B is not reduced directly by Q_A^- such that another electron donor, which might be the Fe-complex, should be involved. To investigate the role of the Fe-complex in the ET proess from Q_A to Q_B, we calculated $E_m(Q_{A/B})$ in the Fe-depleted bRC. By solving the linearized Poisson–Boltzmann (LPB) equation, we account for all amino acids, redox-active cofactors and their different charge states.

2. Computational procedures

2.1. Atomic coordinates and charges

We used the crystal structure of the bRC from *Rhodobacter sphaeroides* for WT-bRC (PDB 1AIG) [4]. Atomic coordinates were obtained in the same way as in previous applications [5]. The positions of hydrogen atoms were energetically optimized with CHARMM [6] using the CHARMM22 force field. During this procedure, the positions of all non-hydrogen atoms were fixed, and all titratable groups were kept in their standard charge state, i.e. basic groups including His were considered to be protonated and acidic groups to be ionized. The coordinates of all atoms available in the crystal structure were not optimized.

Atomic partial charges of the amino acids were adopted from the all-atom CHARMM22 [6] parameter set. For cofactors and residues whose charges are not available in CHARMM22, we used atomic partial charges from previous applications [5].

2.2. Structural model for the Fe-depleted bRC

The crystal structure for the Fe-depleted bRC is not available yet. Depletion of Fe^{2+} from the Fe-complex in WT-bRC may lead to structural changes nearby. However, the replacement of the Fe^{2+} by transition metals (including also

*Corresponding author. Fax: +49 30 83856921.
E-mail addresses: hiro@chemie.fu-berlin.de (H. Ishikita), knapp@chemie.fu-berlin.de (E.-W. Knapp).

[1] Present address: Department of Chemistry, The Pennsylvania State University, 104 Chemistry Building, University Park, PA 16802, USA.

0014-5793/$32.00
doi:10.1016/j.febslet.2006.07.023

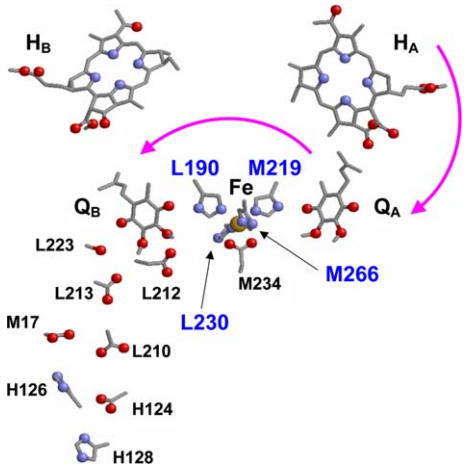

Fig. 1. Location of the Fe-complex in bRC. Pink arrows indicate the direction of the forward ET.

Fe^{2+}), via depletion of the Fe^{2+}, did not essentially affect the ET rates from H_A to Q_A and Q_A to Q_B [2]. This reversibility of the Fe-depletion procedure implies that the structural change accompanied is also reversible and sufficiently small not to affect the ET rates of bRC. Thus, to model the structure for the Fe-depleted bRC, we removed the atomic coordinate of Fe^{2+} in the WT-bRC structure [4] and redefined the ligating residues, four His and one Glu that were originally non-titratable due to the ligation to the Fe^{2+}, as titratable residues. The atomic coordinates for these residues are the same as those in the WT-bRC structure.

Previous studies [5,7,8] suggested the existence of two conformers for Ser-L223 in terms of the hydroxyl group (for the location, see Fig. 1). In one conformer Ser-L223 forms an H bond with the Q_B carbonyl oxygen distant from the non-heme iron complex while in the other Ser-L223 forms an H bond with a carboxyl oxygen of Asp-L213. Since these two conformers resulted in an $E_m(Q_B)$ difference of ~50 mV, we investigated these two conformers independently in the present study [5].

2.3. Computation of protonation pattern and redox potential

The computation of the energetics of the protonation pattern is based on the electrostatic continuum model, in which the linearized Poisson *N* Boltzmann (LPB) equation is solved by the program MEAD from Bashford and Karplus [9]. To sample the ensemble of protonation patterns by a Monte Carlo method, we used our own program Karlsberg (Rabenstein, B. (1999) *Karlsberg online manual*, http://agknapp.chemie.fu-berlin.de/karlsberg/). The dielectric constant was set to $\varepsilon_P = 4$ inside the protein and $\varepsilon_W = 80$ for solvent and protein cavities corresponding to water (for further discussion about the dielectric constants, see supplementary material). All computations were performed at 300 K, pH 7.0 and an ionic strength of 100 mM, if not otherwise specified. The LPB equation was solved by a three-step grid-focusing procedure with a starting grid resolution of 2.5 Å, an intermediate grid resolution of 1.0 Å, and a final grid resolution of 0.3 Å. Monte Carlo sampling yielded probabilities $[A_{ox}]$ and $[A_{red}]$ of the redox states of A. An equal amount of both redox states ($[A_{ox}] = [A_{red}]$) was obtained with a bias potential whose value yielded the midpoint redox potential E_m. Computed E_m are given with milllivolts accuracy, without implying that the last digit is significant. To obtain the absolute value of E_m for a redox-active group in the protein, we calculated the electrostatic energy difference between the two redox states of that group in protein and for a suitable reference model system. The shift of E_m between protein and reference system based on electrostatic energy computations was then added to the measured E_m value for the reference system.

3. Results and discussion

3.1. $E_m(Q_A)$ in Fe-depleted bRC

The calculated $E_m(Q_A)$ in Fe-depleted bRC is significantly lower, by ~210 mV, than that in the WT-bRC (Table 1, Fig. 2). In spectroscopic studies, Fe-depleted bRC showed a 20-fold increase in the life time of the $P^+H_A^-$ state and a corresponding 50% decrease in the yield of the intermediate product state $P^+Q_A^-$ [1]. For WT-bRC, it was reported that the yield of $P^+Q_A^-$ is essentially 100%. Thus, formation of triplet state was observed specifically in the Fe-depleted bRC [1,2].

The correlation of the $E_m(Q_A)$ level with triplet yield was established in a number of studies in photosystem II (PSII). Note that the D1/D2 protein in PSII resembles considerably subunit L/M in bRC [10]. The downshift in $E_m(Q_A)$ decreases the E_m difference between H_A and Q_A, reducing the driving-energy of the corresponding ET process and leading to the charge recombination of the $P^+H_A^-$ state and triplet formation in PSII

Table 1
Calculated $E_m(Q_{A/B})$ for WT-bRC and Fe-depleted bRC in millivolt units

		E_m (Q_A)	E_m (Q_B)	ΔE_m
Ser-L223-H···O=Q_B[a]	Fe-depleted bRC	−386	−205	−181
	WT-bRC	−170	−129	−41
Ser-L223-HO···Asp-L213[b]	Fe-depleted bRC	−378	−302	−76
	WT-bRC	−168	−237	+69

[a]The bRC conformer with an H bond between Ser-L223 and Q_B.
[b]The bRC conformer with an H bond between Ser-L223 and Asp-L213.

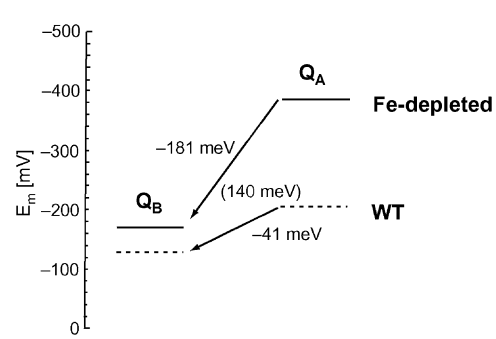

Fig. 2. Driving energy for the ET from Q_A^- to Q_B in WT- and Fe-depleted bRC in [meV]. The value in the bracket refers to the driving-energy difference between WT and Fe-depleted bRC.

(reviewed in Ref. [11]). An upshift of $E_m(Q_A)$ by ~140 mV in PSII is known to be sufficient to minimize the triplet formation [12,13].

Fe depletion may downshift also $E_m(H_A)$. Based on the Fe depleted bRC model the computed downshift in $E_m(H_A)$ is less than 40 mV. Even if we take this downshift in $E_m(H_A)$ into account, the E_m difference between H_A and Q_A in the Fe depleted bRC is by 170 mV smaller than that in WT-bRC. This considerably smaller E_m difference between H_A and Q_A in Fe depleted bRC can enhance triplet yield significantly.

For the mechanism of the decrease in the ET rate upon Fe depletion, (i) structural modulation, (ii) shift of $E_m(Q_A)$, or (iii) change of vibronic coupling between H_A and Q_A were formerly proposed [1]. The present study strongly suggests that the shift of the $E_m(Q_A)$ is the most plausible reason for the decrease in the ET rate upon depletion of the Fe. The fact that the Fe is not on the ET pathway between H_A and Q_A also supports the predominant role of the Fe electrostatics above the other mechanisms on the ET kinetics. We conclude that the existence of the Fe-complex in bRC and PSII is necessary for efficient forward ET from H_A^- to Q_A and suppression of triplet formation by upshifting the $E_m(Q_A)$ with respect to $E_m(H_A)$ to generate a significant energy barrier for the backward ET from Q_A^- to H_A. Under strong illumination, triplet state suppression is particularly important as photoprotection.

3.2. $E_m(Q_B)$ in Fe-depleted bRC

The calculated $E_m(Q_B)$ in the Fe-depleted bRC is by ~70 mV lower than that in WT-bRC. Together with the downshift of ~210 mV in $E_m(Q_A)$, this results in an increased driving-energy for the ET from Q_A^- to Q_B by ~140 meV relative to the WT-bRC (Table 1, Fig. 2). The significantly larger ET driving energy in the Fe-depleted bRC indicates that Fe^{2+} is not necessary to yield a large E_m difference between Q_A and Q_B for exergonic ET. In turn, Fe^{2+} constrains the E_m difference to a smaller E_m range in WT-bRC. Based on ET rates for charge recombination between Q_A^-/Q_B^- and P^+, Debus et al. [2] estimated an increase of up to 100 meV in ET driving-energy upon depletion of Fe^{2+}, which is essentially consistent with our value of ~140 meV. From the empirical equation of Page et al. [14], we estimate the characteristic time for the ET from Q_A^- to Q_B in Fe depleted bRC to be 2 μs (with reorganization energy $\lambda = 0.85$ eV [15]), which is sufficiently small relative to 350 μs for kinetic phase 1 in the Fe depleted bRC [2], i.e. the rate-limiting step is not the ET but the conformational gating step as in WT-bRC [16]. From this estimate we conclude that the first ET in Fe depleted bRC is also independent of the ET driving energy (i.e. E_m difference between Q_A and Q_B).

The question arises why the calculated downshift in $E_m(Q_A)$ is by ~140 mV larger than that in $E_m(Q_B)$ in spite of the pseudo-C_2 symmetry in the $Q_{A/B}$ positions with respect to the Fe-complex (see Fig. 1). As expected from the structural symmetry, the direct influences of the Fe^{2+} charge in WT-bRC on $E_m(Q_A)$ and $E_m(Q_B)$ that is computed for a fixed protonation pattern are essentially the same, yielding upshifts of +186 and +169 mV for $E_m(Q_A)$ and $E_m(Q_B)$, respectively (Table 2). In turn, this indicates that changes in protonation pattern of titratable residues in the Fe-depleted bRC are the main factors that increase the E_m difference between Q_A and Q_B with respect to the WT-bRC. Especially, contributions of protonation pattern changes upon Fe depletion to E_m (Q_B) are significant, resulting in an upshift of 94 mV for $E_m(Q_B)$ (Table 2). Hence, if the protonation pattern of titratable residues did not change upon Fe depletion, the calculated $E_m(Q_B)$ of −205 mV in Fe-depleted bRC would be 94 mV lower. Indeed, in the Fe depleted bRC, we observed changes in the protonation pattern of His residues. His-L230, His-M219 and His-M266 become protonated by ~0.4 H^+ upon formation of Q_A^- while His-L190, His-L230 and His-M266 protonate by ~0.3–0.5 H^+ upon formation of Q_B^-. In WT-bRC, all four His are ligands to the Fe-complex and therefore not allowed to change their protonation states.

Table 2
Contributions to $E_m(Q_{A/B})$ for WT-bRC[a] and Fe depleted bRC[a] in millivolt units

	$E_m(Q_A)$	$E_m(Q_B)$	ΔG[b]
E_m in Fe-depleted[a]	−386	−205	−181
(influence of protonation shift from native)	(−30)	(+93)	(−123)
E_m in Fe-depleted[a] without protonation change from native	−356	−298	−58
(direct influence of Fe^{2+} in native)	(+186)	(+169)	(+17)
E_m in native[a]	−170	−129	−41

[a]The bRC conformer with an H bond between Ser-L223 and Q_B.
[b]$\Delta G = E_m(Q_A) - E_m(Q_B)$.

In the absence of these protonation pattern changes, the E_m difference between Q_A and Q_B is 58 mV, which is almost the same difference as that for the WT-bRC (Table 2). The much larger E_m modulation of Q_B with protonation pattern changes is obviously due to the existence of the cluster of titratable residues in the Q_B side (for these residues, see the review [17]). Thus, we conclude that the computed increase of the E_m difference between Q_A and Q_B, which was also suggested from kinetic studies [2], is due to significant contributions of the accompanied protonation pattern changes near Q_B, upshifting $E_m(Q_B)$.

To compensate for the change in the net charge of bRC arising with Fe release the titratable residues may change their protonation states. Hereby, the direct influence of the originally induced net charge is weakened by protonation pattern changes (i.e. indirect influence). A similar important contribution of the indirect electrostatic influence was observed also upon mutations. In bRC, proton transfer to Q_B was inhibited upon the E(L212)A/D(L213)A double mutant but could be recovered by an additional single mutation, either R(M231)L or N(M43)D, being 9–15 Å away from Q_B [18]. The altered pH-dependence of the equilibrium constant for the ET $Q_A^-Q_B \leftrightarrow Q_AQ_B^-$ implies such a change of protonation states. As a result, changes of protonation pattern altered the $E_m(Q_B)$ by 24–45 mV, even though the mutational site is at a considerably distance from Q_B [18]. Hence, the protonation pattern change play an important role in determining the energetics of redox-active protein cofactors especially if the protein possesses a large number of titratable residues.

4. Conclusion

The presence of Fe^{2+} or other divalent metal ions upshift $E_m(Q_A)$ considerably, which plays a significant role in both facilitating ET from H_A^- to Q_A and reducing triplet formation. The E_m difference between Q_A and Q_B is much larger in Fe-depleted bRC than in WT-bRC, indicating that Fe^{2+} is not necessary to render the ET processes between Q_A^- and Q_B sufficiently exergonic.

Acknowledgements: We are grateful for valuable discussions with Dr. Michael Haumann. We thank Dr. Donald Bashford and Dr. Martin Karplus for providing the programs MEAD and CHARMM22, respectively. This work was supported by the Deutsche Forschungsgemeinschaft SFB 498, Project A5, Forschergruppe Project KN 329/5-1/5-2, GRK 80/2, GRK 268, GRK 788/1.

Appendix A. Supplementary data

Supplementary data associated with this article can be found, in the online version, at doi:10.1016/j.febslet.2006.07.023.

References

[1] Kirmaier, C., Holten, D., Debus, R.J., Feher, G. and Okamura, M.Y. (1986) Primary photochemistry of iron-depleted and zinc-reconstituted reaction centers from *Rhodopseudomonas sphaeroides*. Proc. Natl. Acad. Sci. USA 83, 6407–6411.

[2] Debus, R.J., Feher, G. and Okamura, M.Y. (1986) Iron-depleted reaction centers from *Rhodopseudomonas sphaeroides* R-26.1: characterization and reconstitution with Fe^{2+}, Mn^{2+}, Co^{2+}, Ni^{2+}, Cu^{2+}, and Zn^{2+}. Biochemistry 25, 2276–2287.

[3] Remy, A. and Gerwert, K. (2003) Coupling of light-induced electron transfer to proton uptake in photosynthesis. Nat. Struct. Biol. 10, 637–644.

[4] Stowell, M.H.B., McPhillips, T.M., Rees, D.C., Solitis, S.M., Abresch, E. and Feher, G. (1997) Light-induced structural changes in photosynthetic reaction center: implications for mechanism of electron–proton transfer. Science 276, 812–816.

[5] Ishikita, H. and Knapp, E.-W. (2004) Variation of Ser-L223 hydrogen bonding with the Q_B redox state in reaction centers from *Rhodobacter sphaeroides*. J. Am. Chem. Soc. 126, 8059–8064.

[6] Brooks, B.R., Bruccoleri, R.E., Olafson, B.D., States, D.J., Swaminathan, S. and Karplus, M. (1983) CHARMM: a program for macromolecular energy minimization and dynamics calculations. J. Comput. Chem. 4, 187–217.

[7] Alexov, E.G. and Gunner, M.R. (1999) Calculated protein and proton motions coupled to electron transfer: electron transfer from Q_A^- to Q_B in bacterial photosynthetic reaction centers. Biochemistry 38, 8253–8270.

[8] Paddock, M.L., Flores, M., Isaacson, R., Chang, C., Selvaduray, P., Feher, G. and Okamura, M.Y. (2005) Hydrogen bond reorientation upon Q_B reduction revealed by ENDOR spectroscopy in reaction centers from *Rhodobacter sphaeroides*. Biophys. J. 88, 204A.

[9] Bashford, D. and Karplus, M. (1990) pK_as of ionizable groups in proteins: atomic detail from a continuum electrostatic model. Biochemistry 29, 10219–10225.

[10] Michel, H. and Deisenhofer, J. (1988) Relevance of the photosynthetic reaction center from purple bacteria to the structure of photosystem II. Biochemistry 27, 1–7.

[11] Rutherford, A.W. and Krieger-Liszkay, A. (2001) Herbicide-induced oxidative stress in photosystem II. Trends Biochem. Sci. 26, 648–653.

[12] Krieger, A. and Weis, E. (1992) Energy dependent quenching of chlorophyll a fluorescence: the involvement of proton–calcium exchange at photosystem II. Photosynthetica 27, 89–98.

[13] Krieger, A., Rutherford, A.W. and Johnson, G.N. (1995) On the determination of redox midpoint potential of the primary quinone electron transfer acceptor, Q_A, in photosystem II. Biochim. Biophys. Acta 1229, 193–201.

[14] Page, C.C., Moser, C.C., Chen, X. and Dutton, P.L. (1999) Natural engineering principles of electron tunnelling in biological oxidation–reduction. Nature 402, 47–52.

[15] Li, J., Takahashi, E. and Gunner, M.R. (2000) $-\Delta G^0_{AB}$ and pH dependence of the electron transfer from $P^+Q_A^-Q_B$ to $P^+Q_AQ_B^-$ in *Rhodobacter sphaeroides* reaction centers. Biochemistry 39, 7445–7454.

[16] Graige, M.S., Feher, G. and Okamura, M.Y. (1998) Conformational gating of the electron transfer reaction $Q_A^-Q_B \rightarrow Q_AQ_B^-$ in bacterial reaction centers of *Rhodobacter sphaeroides* determined by a driving force assay. Proc. Natl. Acad. Sci. USA 95, 11679–11684.

[17] Okamura, M.Y., Paddock, M.L., Graige, M.S. and Feher, G. (2000) Proton and electron transfer in bacterial reaction centers. Biochim. Biophys. Acta 1458, 148–163.

[18] Sebban, P., Maróti, P., Schiffer, M. and Hanson, D.K. (1995) Electrostatic dominoes: long distance propagation of mutational effects in photosynthetic reaction centers of *Rhodobacter capsulatus*. Biochemistry 34, 8390–8397.